

PREDICTION OF TOPOGRAPHIC CHANGES ON ENSHU-NADA COAST CONSIDERING EFFECT OF BOTH WAVES AND WINDBLOWN SAND

Takuya Yokota¹, Takaaki Uda², Akio Kobayashi³ and Yasuhito Noshi³

The morphology of sand dunes formed on the Maisaka and Hamamatsu coasts facing the Enshu-nada Sea was investigated by field observation. The development of sand dunes was numerically predicted using a model predicting the effect of both waves and windblown sand. In the field observation, the development of sand dunes with a rhythmic shape similar to a sand spit was observed in the backshore area. It was found that pine trees died in the area with a narrow sand dune owing to wave run-up and the dispersion of salinity during storm wave conditions. In the numerical simulation, the formation of sand dunes was successfully reproduced under the condition that the predominant wind blew at a large angle relative to the direction normal to the shoreline.

Keywords: windblown sand; sand dune; cellular automaton method; Maisaka coast; Hamamatsu coast

INTRODUCTION

In Japan, there are a number of coasts where a large amount of windblown sand is transported. In particular, on coasts facing the Pacific Ocean and formed by the deposition of sand supplied from large rivers, the amount of windblown sand is significant in winter. A coastal sand dune can be formed as a result of the transport of windblown sand on coasts composed of fine and medium-size sand. These coastal sand dunes prevent the inundation of seawater and the diffusion of salinity inland during tsunamis or typhoons, and serve as a natural barrier protecting the coastal roads and residential areas behind the coastline. On the Hamamatsu coast facing the Pacific Ocean, as shown in Fig. 1, several coastal sand dunes have formed owing to windblown sand in winter. In particular, the Nakatajima sand dune formed immediately west of the Magome River is famous. Junaidi et al. (2009) successively monitored the changes in the topography of this sand dune and studied the relationship between the short-term

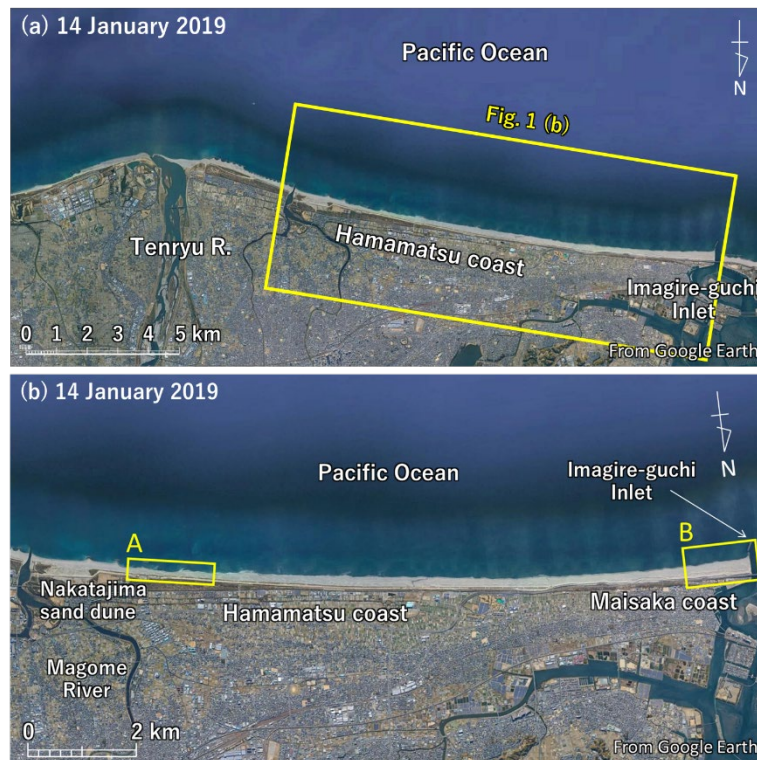


Figure 1. Satellite image of area between Tenryu River mouth and Imagire-guchi Inlet.

¹ Coastal Engineering Laboratory Co., Ltd., 1-22-301 Wakaba, Shinjuku, Tokyo 160-0011, Japan

² Public Works Research Center, 1-6-4 Taito, Taito, Tokyo 110-0016, Japan

³ Department of Oceanic Architecture & Engineering, College of Science & Technology, Nihon University, 7-24-1 Narashinodai, Funabashi, Chiba 274-8501, Japan

topographic changes of the sand dune and windblown sand. Sato (2008) analyzed the topographic changes caused by the movement of sediment supplied from the Tenryu River and windblown sand. In the prediction of beach changes of this coast, the combined effect of waves and windblown sand must be considered. In this study, the topography of coastal sand dunes on coasts facing the Enshu-nada Sea was measured and topographic changes were calculated using a model for predicting the effect of both waves and windblown sand; the model was developed by Yokota et al. (2022), with which they predicted the topographic changes due to the effect of both waves and windblown sand.

GENERAL CONDITION OF STUDY AREA

The areas A and B shown in Fig. 1 were set on the Hamamatsu and Maisaka coasts, respectively, and the formation of coastal sand dunes behind the shoreline and their surrounding conditions were investigated by field surveys. Figure 2 shows an enlarged satellite image of area A (Hamamatsu coast) in Fig. 1. The fluvial sediment from the Tenryu River is transported westward along the coast by longshore sand transport (Ishikawa et al., 2019), and erosion has occurred owing to the decrease in sediment supply from the Tenryu River. For this reason, on the west side of the Magome River mouth, beach nourishment with coarse materials has been carried out as a measure against erosion, as well as the installation of three offshore breakwaters (Uda et al., 2014). In this area, pine tree forest extends along the coastline and a tsunami dike has been constructed. Moreover, many sand dunes, indicated by D1 to D6 in Fig. 2, develop between the shoreline and the coastal forest.

Figure 3 shows the wind rose in this area ($34^{\circ}39'43.29''\text{N}$, $137^{\circ}43'37.96''\text{E}$) obtained from NEDO NeoWinds along with the overall mean shoreline (dashed line). The WNW direction, which is the prevailing wind direction in this area, almost coincides with the direction of the coastline. Wind blows along the shoreline almost from the right side; thus, sand dunes are formed by the action of this wind.



Figure 2. Enlarged satellite image of study area A.

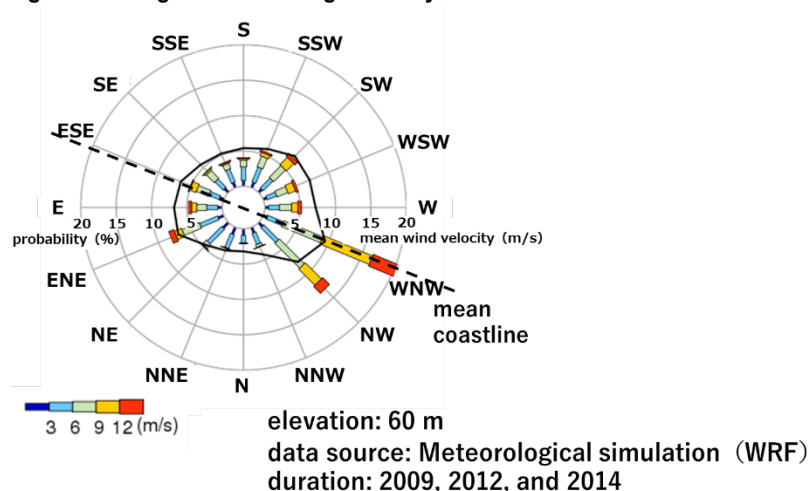


Figure 3. Wind rose in study area (NEDO NeoWinds).



Figure 4. Enlarged satellite image of study area B.

Figure 4 shows an enlarged satellite image of area B (Maisaka coast) around Imagire-guchi Inlet, as shown in Fig. 1 and the location where the photographs were taken. On this coast, part of the westward longshore sand transport is blocked by a training jetty at Imagire-guchi Inlet. Sand carried by longshore sand transport is deposited offshore owing to the blockage caused by the ebb tidal current at Imagire-guchi Inlet, then turns westward and reaches downcoast (the Arai coast) on the west side of the inlet. On the other hand, since the northwesterly wind prevails in winter in this area, sand deposited on the east side of the training jetty is transported toward southeast. When considering the sand budget near the left bank of the training jetty, sand is supplied to the beach by the action of waves at the amount equivalent to that carried away by the windblown sand, resulting in a clockwise circulation of sand movement caused by waves and windblown sand. It is assumed that the shoreline configuration has been maintained owing to this phenomenon.

Field observation in areas A and B was carried out on 10 December 2019. In addition, in area A, the X -axis is set in the longshore direction and the Y -axis is set perpendicular to the X -axis, as shown in Fig. 2. Moreover, images were taken using a UAV (drone Matrice 210 RTK V2) in area A.

RESULTS OF FIELD OBSERVATIONS

(1) Hamamatsu coast

Figure 5 shows an aerial photograph of the study area including D1–D6 with arrows indicating where the color of the pine trees changed from green to brown owing to the diffusion of salinity under storm wave conditions. The shoreline in this area protruded near $X = 200, 625,$ and $1,100$ m owing to the formation of longshore sandbars, and the wavelength of the shoreline undulation was 450 m between the shoreline protrusions **a** and **b** with an amplitude of 40 m. D1–D6 have formed behind the shoreline within a longshore distance of $1,200$ m, resulting in the wavelength of 200 m, which accounts for 44% of the wavelength of the longshore shoreline undulation.

In Fig. 5(a), the color of the coastal forest behind the coastal sand dunes locally changed from green to brown. This is because the diffusion of salinity occurred during Typhoon 1919 that hit the area on October 12, 2019. Figure 5(b) shows the contours of the sand dunes produced from the imagery taken with a UAV. The intervals of the contours are narrow, forming a steep slope where the embayment shoreline is located close to the seaward protrusion of the coastal sand dunes. The elevation of the sand dunes is approximately 6 m above MSL, and these coastal sand dunes are rhythmically arranged along the shoreline. When examining the shape of D2 in detail, a narrow sand deposition zone extends eastward along the seaward marginal line of the sand dune with a concave trough landward of the sand dune. This shape of the topography resembles that of a single sand spit formed by waves. Furthermore, a steep slope has been formed along the seaward side of the coastal sand dunes owing to erosion by waves during Typhoon 1919. The width of D2 significantly varied alongshore: 0 m at the east end because of the lack of sand dunes, 40 m at the central part, and 10 m between D2 and D3. Because eastward (leftward in the figure) windblown sand prevails along the coastline, the shape of all the coastal sand dunes was asymmetric in the east–west direction.

Figure 6 shows the summary of the shoreline, the seaward boundary of the coastal forest area, the seaward marginal line of the coastal forest, and the contour with $+5$ m above MSL. When comparing the

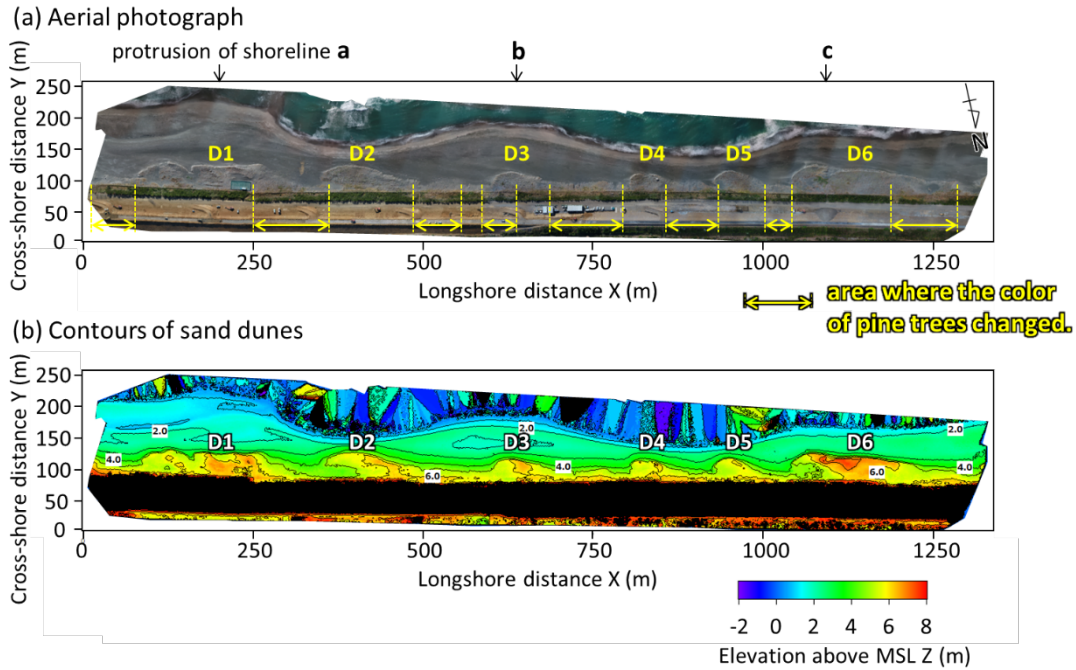


Figure 5. Aerial photograph of study area taken by UAV and contours around sand dunes D1–D6.

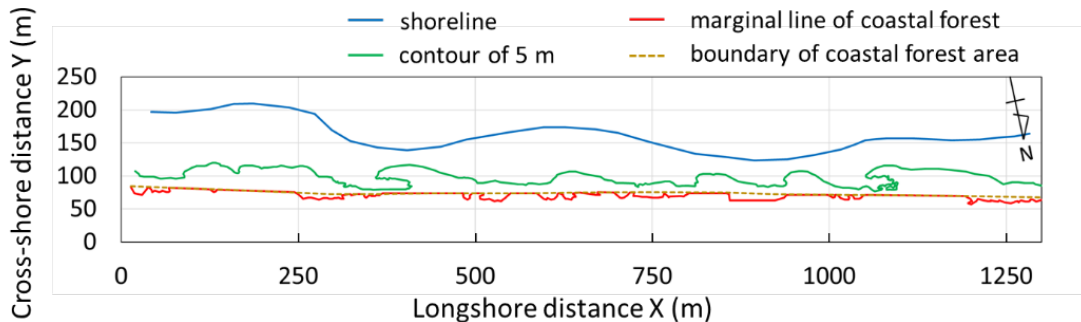


Figure 6. Shoreline, seaward boundary of the coastal forest area, seaward marginal line of coastal forest, and contour of +5 m height.

seaward marginal line of the coastal forest and the contour of +5 m height, the marginal line of the coastal forest recedes in the area with a narrow beach in front of the coastal forest, but not in the area with a wide beach. In particular, the recession of the marginal line of the coastal forest is significant in the vicinity of $X = 850$ m where a concave shoreline has been formed. In contrast, the marginal line of the coastal forest is prevented from receding in the area, such as the vicinity of $X = 350$ m, where the width of the sand dune is large in front of the coastal forest, even though the shoreline is of concave shape. This is because the sand dune in front of the coastal forest functioned as a natural levee against storm waves; wave run-up and the diffusion of salinity inland were prevented in the area with a sufficiently wide sand dune.

Dune conditions were observed at Sts. 1–6 located between D4 and D5 and in the vicinity of D2, as shown in Fig. 2. On 12 October 2019, storm waves associated with Typhoon 1919 hit this area, and waves ran up on the sand dunes, resulting in the erosion of the seaward part of the sand dunes. After the typhoon, traces of wave run-up and erosion remained at many locations. Figure 7(a) shows the traces of return flow of run-up waves at the east corner of D5. Since this area is located between D4 and D5 and open to the sea, storm waves ran up to the wooden fence constructed along the coastal forest to prevent the transport of windblown sand. As seen in Fig. 7(a), D5 was eroded by the return flow of the run-up waves that deeply invaded the backshore. Since the ground elevation was small between D4 and D5, the diffusion of salinity was significant, and fewer pine trees grew in this area than in the adjacent area. Figure 7(b) shows the traces of the return flow from the sand dune at St. 2 behind D4. Almost all the pine

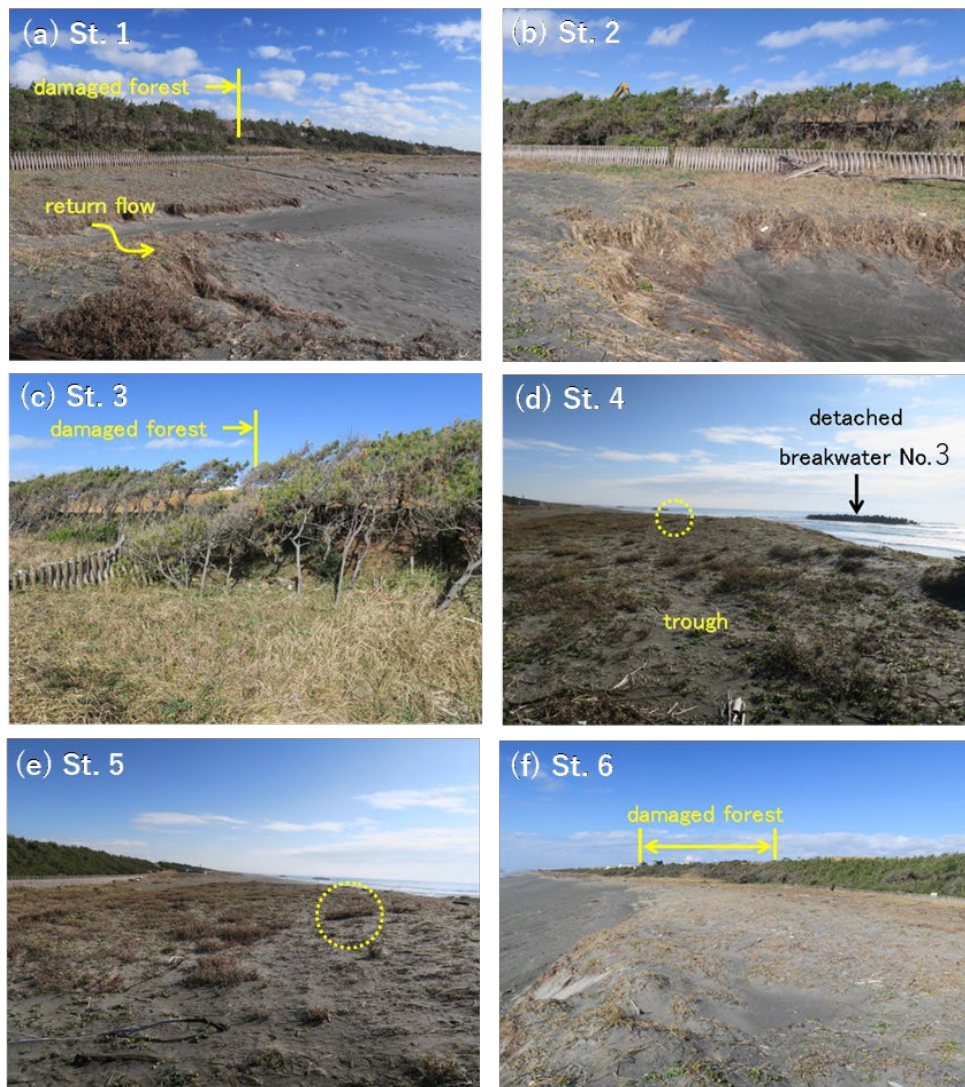


Figure 7. Photographs at Sts. 1–6 shown in Fig. 2.

trees were dead in this vicinity, because much salinity is assumed to be transported from the sea because of the concave topography on the backshore.

Figure 7(c) shows pine trees at the west end of D2. In the western half, the density of pine trees was lower than that in the eastern half behind D2. Figure 7(d) shows the central part of D2 and detached breakwater No. 3 at a far distance, viewed from the west side of D2. A low ridge was formed along the seaward end of D2 with a trough behind the ridge. The surfaces of the ridge and trough were covered with fine sand, whereas dune vegetation such as *Carex kobomugi* grew well in the eastern half of the sand dune. Figure 7(e) shows the enlarged view of the central part of D2, facing east, where the circle in Fig. 7(e) is drawn at the same location as that in Fig. 7(d) for easy comparison. Immediately west of the vegetation zone, active sand movement was observed on the sand dune with a gradual landward slope. The photograph in Fig. 7(f), taken from St. 6 shows the upwind side of D2. Sand has been transported over the west ridge of D2 thereby increasing the sand dune height. The surface of the sand dune in this area was covered with *Carex kobomugi*. Owing to the sand trapping effect of the vegetation, small sand mounds were formed on the sand dune.

(2) Maisaka coast

In the survey area, a slightly elevated mound was formed owing to an artificial embankment. Figure 8(a) shows this mound viewed in the southwest direction. Here, vegetation traps windblown sand that has developed under the action of wind from the northwest, forming numerous small sand dunes. At the eastern end of this dune, a steep slope was formed, and the sand that was transported eastward was deposited toward the center, forming a barchan (Fig. 8(b)). On the other hand, Fig. 8(c) shows a

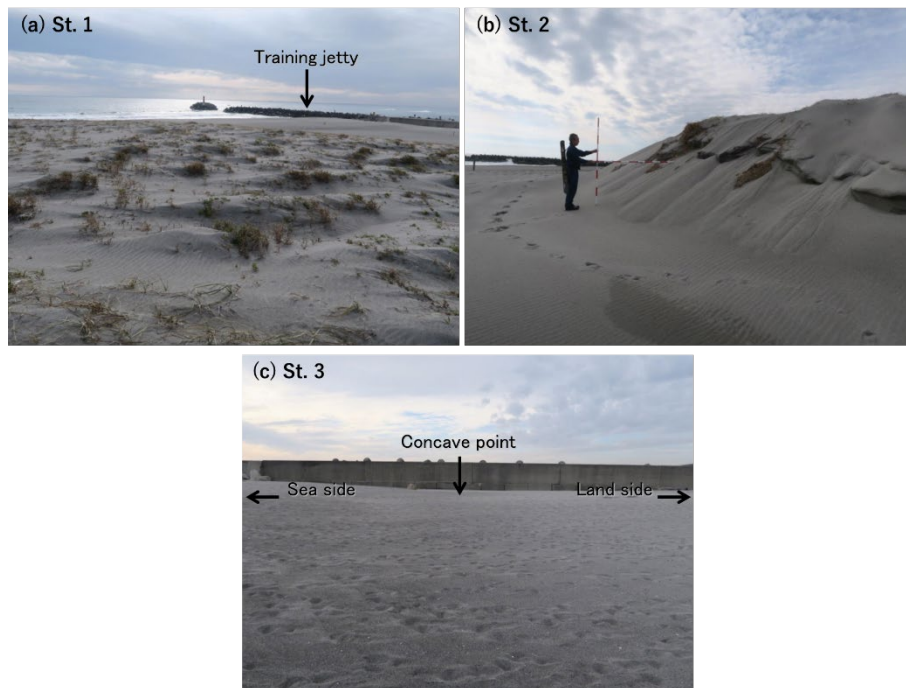


Figure 8. Photographs at Sts. 1–3 shown in Fig. 4.



Figure 9. Aerial photograph of Maisaka coast taken by UAV.

photograph of sand deposition on the east side of the training jetty. When examining the shape of the boundary between the training jetty and the beach, it was found that the ground level decreased landward from the berm, and then the elevation increased landward again. Figure 9 shows a UAV image of the Maisaka coast in area B. In this area, the beach width is wide and several sand dunes have randomly formed on the backshore.

MODEL

The calculation of beach changes and sand dune formation on the backshore was carried out using a model developed by Yokota et al. (2022) for predicting three-dimensional (3-D) beach changes under combined actions of waves and wind. In this model, the beach changes due to waves occurring in the depth zone between the depth of closure (h_c) and the berm height (h_R) are predicted using the BG model (a model for predicting three-dimensional beach changes based on Bagnold's concept) (Uda et al., 2018), whereas topographic changes due to windblown sand in the area landward of a berm top are predicted by a cellular automaton method. In the calculation of windblown sand by the cellular automaton method, the two most important processes, saltation and avalanche, are taken into account (Katsuki and Kikuchi, 2006).

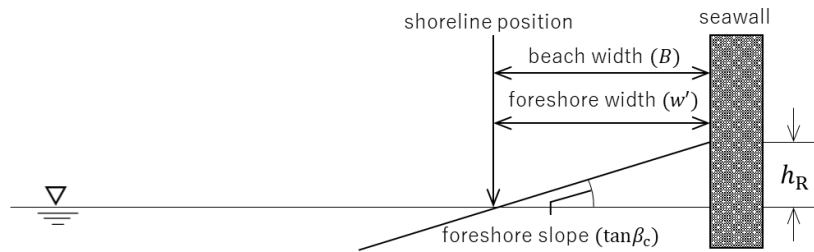
Two-dimensional meshes were taken on Cartesian coordinates (x, y) , and the elevation at the mesh point was set as $z(x, y, t)$. We assumed that the mesh size is sufficiently larger than the size of sand particles. The saltation distance L_s was determined using Eq. (1) on the basis of the observation results obtained by Andreotti et al. (2002) and is the simplest polynomial expression that can be used to evaluate the obtained results of sand flux on a sand dune including multiphase flow.

$$L_s = L \left[1.0 + b_1 \left(\frac{z}{h} \right) - b_2 \left(\frac{z}{h} \right)^2 \right] \quad (1)$$

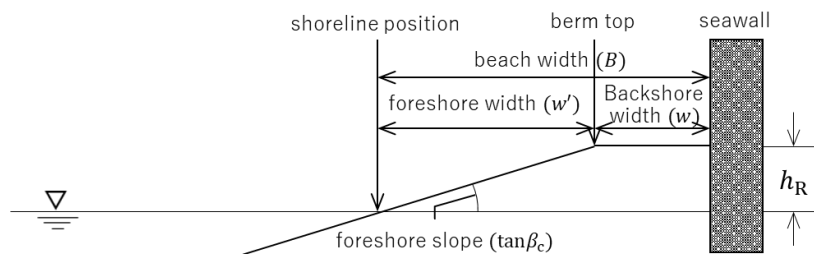
b_1 and b_2 are the coefficients to control sand transport flux, expressed by the product of L_s determined using Eq. (1) and the moving mass of sand. L is a reference distance (here, we choose 1.0 m) and h is the reference height (here, the berm height). Equation (1) shows that the higher the elevation where sand particles are deposited, the longer the distance that the sand particles are transported by wind, but L_s has a limit and the sand flux after its maximum value is reached is regarded as a constant, and no decreasing functional form is employed. When there is an obstacle in the field, no saltation is assumed, because a vortex is formed behind an obstacle owing to the separation of the flow (Pye and Tsoar, 1990). Originally, the sand flux is given by the product of the moving mass and L_s , and the sand flux can be expressed by Eq. (1) when the wind velocity is constant, assuming that the moving mass is constant. When the wind velocity changes, the coefficient in Eq. (1) can be changed depending on the wind velocity. To combine the BG model and the cellular automaton method, the calculation domains were separated at the berm location, assigning the landward region of the berm as the domain of windblown sand.

The rate of windblown sand is assumed to attain equilibrium at a location distant from the starting point for the approach run in the downwind direction. Here, the conditions of windblown sand occurrence were defined, as shown in Fig. 10, depending on the backshore width, assuming that the minimum

(a) No windblown sand ($B < w'$)



(b) Windblown sand ($0 < w < 10 \text{ m}$)



(c) Windblown sand ($10 \text{ m} < w$)

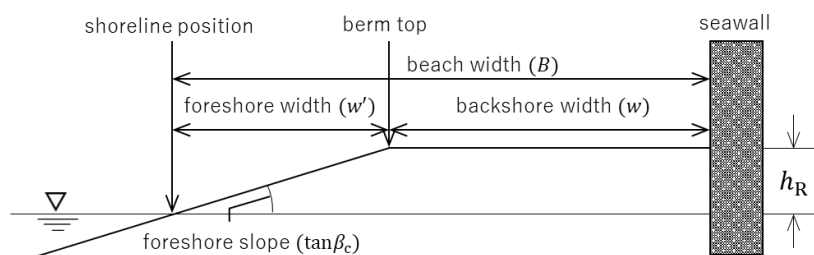


Figure 10. Conditions of windblown sand occurrence.

approach run is 10 m (Horikawa et al., 1983). No windblown sand is transported when the beach width B is smaller than the foreshore width w' ; the moving mass of sand (q) attributable to windblown sand was given by the value multiplied by the coefficient μ determined by solving Eq. (2) when the backshore width w is smaller than 10 m. When w is greater than 10 m, μ is unity.

$$\mu = \frac{1}{2} \left[\cos\left(\frac{\pi}{10}b\right) + 1 \right] \quad (2)$$

CALCULATION OF TOPOGRAPHIC CHANGES

From the observation results, calculations using the BG model (Case 1) and calculations using the model for predicting the effect of both waves and windblown sand (Case 2) were carried out. In the calculation, the initial topography was simplified, given by parallel isolines (Fig. 11). Table 1 shows calculation conditions. Wave height, wave direction, equilibrium slope, the depth of closure h_c , and berm

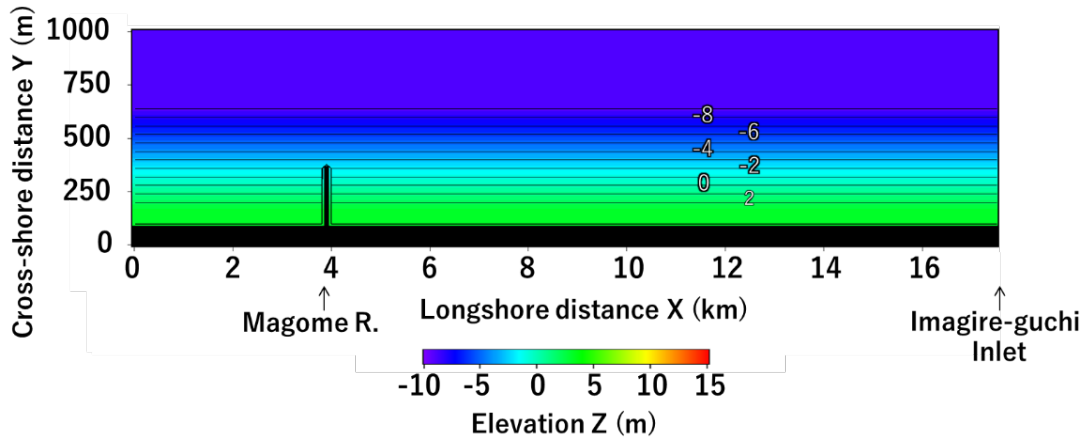


Figure 11. Initial topography for calculation.

Table 1. Calculation conditions.

Calculation Cases		Case 1	Case 2
Equilibrium slope		1/40	
Incident wave conditions	Incident wave height (m)	1.32	
	Wave direction α (deg)	Distributed in the coastal direction from 15° to 9°	
	Water level above MSL (m)	0.0	
Depth range of beach changes	Depth of closure h_c (m)	9.0	
	Berm height h_R (m)	3.0	
Coefficient of longshore sand transport	Coefficient of longshore sand transport	0.2	
	Ratio of cross-shore sand transport relative to longshore sand transport	0.2	
Depth distribution of longshore sand transport		Quadratic equation of the depth by Uda and Kawano (1996)	
Wind direction α_w (deg.) relative to Y-axis			85.0
Moving mass by wind ($m^3/m/yr$)			0.0876
Coefficient of Eq.(1)	b_1 and b_2		50 and 0.5
Critical slope of sand on land and in seabed		1/2	
Calculation domain	Longshore distance x (m)	17500	
	Cross-shore distance y (m)	1000	
Mesh size	Δx (m)	100	
	Δy (m)	20	
Time interval Δt (h)		0.5	
Calculation steps		5.0×10^5	

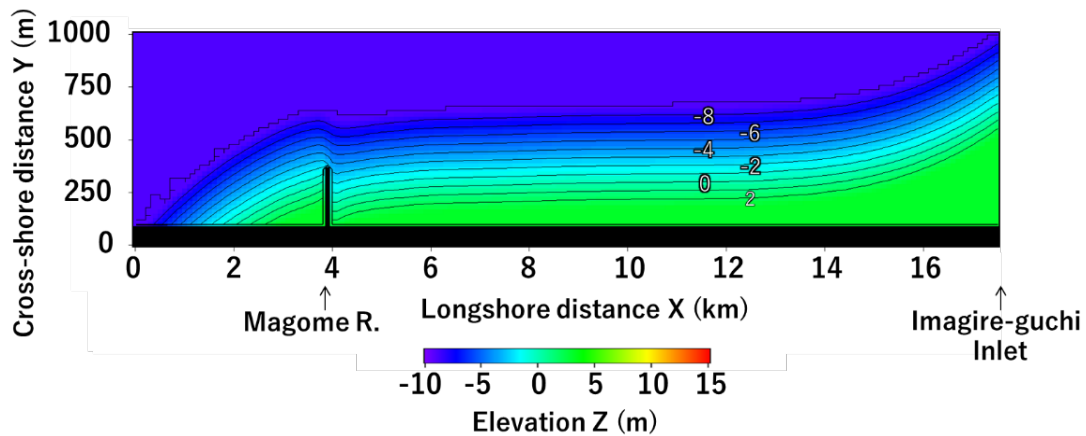


Figure 12. Predicted topography (Case 1).

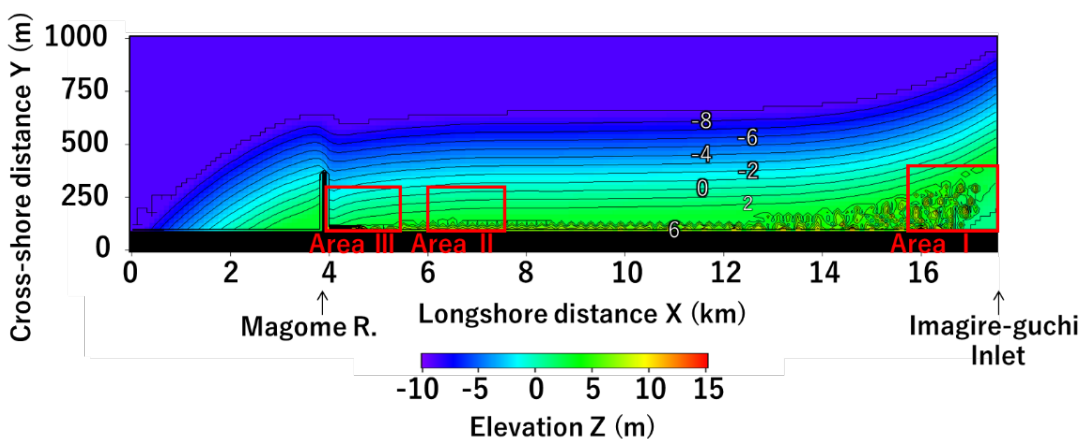


Figure 13. Predicted topography (Case 2).

height h_R are the same as these in previous study (Ishikawa et al., 2019) using the BG model in this domain. The wind was assumed to blow from the direction of 85° clockwise with respect to the direction normal to the initial shoreline. The mass of transported sand, q , was set to be $12.9 \text{ m}^3/\text{m}/\text{yr}$. Figure 12 shows the calculation results of Case 1, in which only westward longshore sand transport is given without considering windblown sand. Since Case 1 does not consider windblown sand, a flat surface with an elevation of 3 m is formed behind the berm and the maximum beach width is 400 m near Imagire-guchi Inlet. Figure 13 shows the calculation results of Case 2 considering windblown sand. Beach changes occurred owing to westward sand transport, as well as the formation of sand dunes due to windblown sand. For the rectangular areas defined as areas I, II, and III from the upwind side in Fig. 13, the results of the calculation in each area are shown in Fig. 14. In area I, a flat surface was formed near the east side of the jetty, and then randomly shaped dunes were formed on the east side; this situation was reproduced by calculation. In area II, sand dunes with a height of 6 m were rhythmically formed at intervals of 200 m along the shoreline, as shown in Fig. 5. Sand dunes with the same characteristics as measured in the field were calculated. In area III, a large amount of windblown sand was deposited to form a sand dune with a height of 11 m, and the formation mechanism of the Nakatajima sand dune, a natural sand dune, was confirmed. Figure 15 shows the topographic changes obtained as the difference between the calculation results of Cases 2 and 1. In the range from $h_c = 9 \text{ m}$ to $h_R = 3 \text{ m}$, where topographic changes occur owing to wave action, the entire area finds to erode owing to sand carried away to the land area. On the other hand, in the area behind the berm on land, the sand that was transported as windblown sand was deposited and sand dunes were formed. Thus, on a coast where the effect of windblown sand is remarkable, part of the sand deposited near the shoreline owing to waves is carried inland as windblown sand, forming sand dunes and thereby decreasing the amount of sand deposited on the seabed.

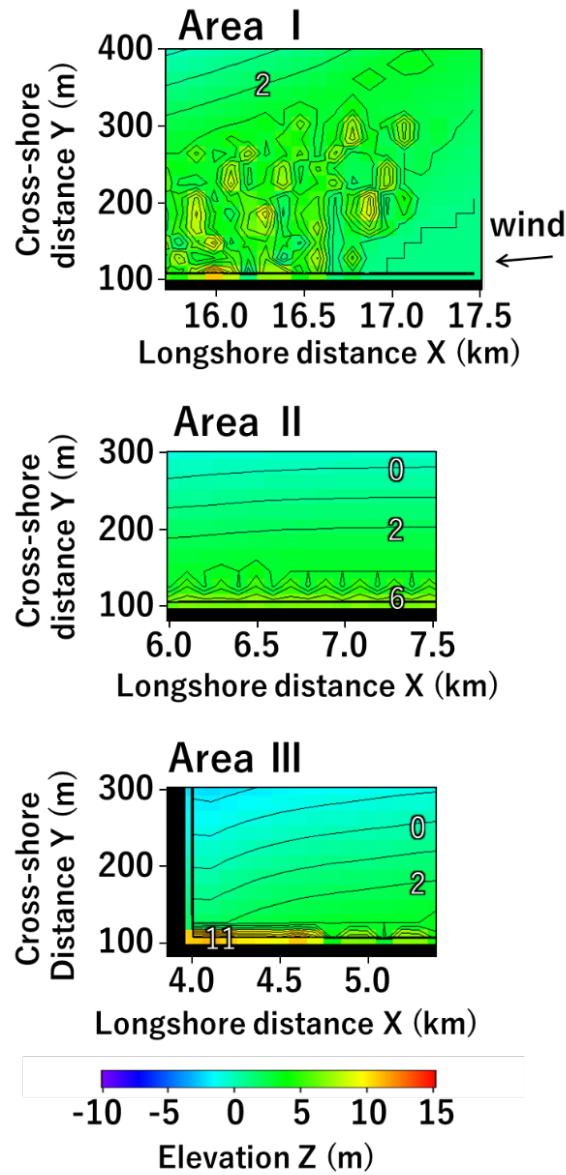


Figure 14. Enlarged view of calculation result of Case 2 in areas I, II, and III.

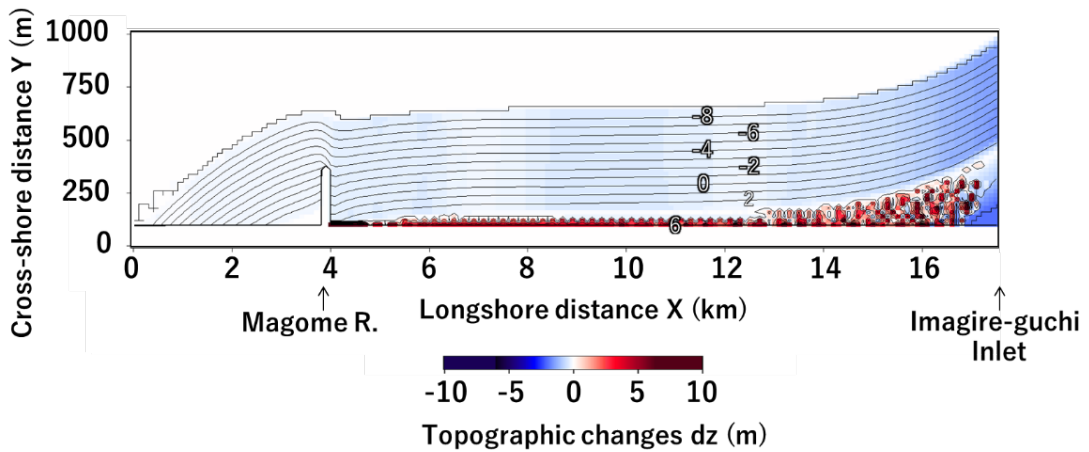


Figure 15. Topographic changes in Cases 2 and 1.

CONCLUSIONS

The morphology of sand dunes formed on the Maisaka and Hamamatsu coasts facing the Enshu-nada Sea was investigated by field observation. The development of sand dunes was numerically predicted using the model predicting the effect of both waves and windblown sand. In the field observation, the development of sand dunes of a rhythmic shape similar to a sand spit was observed in the backshore area. In the numerical simulation, sand dunes were successfully reproduced under the condition that wind blew at a large angle relative to the direction normal to the shoreline. The present model can be used to predict beach changes on a coast subject to the action of both waves and wind.

REFERENCES

- Andreotti, B., Claudin, P., and Douady, S. 2002. Selection of dune shapes and velocities, Part 1: Dynamics of sand, wind and barchans, *Eur. Phys. J.*, B28, 321–339.
- Horikawa, K., Hotta, S., Kubota, S., and Katori, K. 1983. Field observation of windblown sand by trench trap, *J. Jpn. Coastal Eng.*, Vol. 30, 406–410. (in Japanese)
- Ishikawa, T., Uda, T., Furuike, K., Kainuma, M., and Ohashi, Y. 2019. Shore protection effect to west Enshu-nada coast expected by increase in sand supply from Tenryu River, *Proc. JSCEB2 (Coastal Engineering)*, Vol. 75, No. 2, I_577–I_582. (in Japanese)
- Junaidi, Aoki, S., Kato, S., Kataoka, M., Wakae, N., and Amasaki, T. 2009. Characteristics of sediment transport and short-term topographic change on the Nakatajima dune, *Proc. JSCEB2 (Coastal Engineering)*, Vol. 65, No. 1, I_621–I_625. (in Japanese)
- Katsuki, A. and Kikuchi, M. 2006. Simulation of barchan dynamics with interdune sand stream, *RIMS Kokyuroku*, 1472, 67–70. (in Japanese)
- NEDO NeoWinds (Accessed on 10 January 2020).
http://app10.infoc.nedo.go.jp/Nedo_Webgis/index.html
- Pye, K. and Tsoar, H. 1990. Aeolian sand and sand dunes, Unwin Hyman, London, 42–43.
- Sato, S. 2008. Dynamics of sand movement on Hamamatsu coast facing Enshu-Nada, *Proc. JSCEB*, Vol. 64, No. 3, 192–201. (in Japanese)
- Uda, T., Ishikawa, T., Furuike, K., Aoba, Y., and Oido, S. 2014. Reproduction of beach changes after beach nourishment on Hamamatsu-Shinohara coast in Shizuoka Prefecture and its prediction, *Proc. JSCEB2 (Coastal Engineering)*, Vol. 70, No. 2, I_691–I_695. (in Japanese)
- Uda, T., Serizawa, M., and Miyahara, S. 2018. Morphodynamic model for predicting beach changes based on Bagnold's concept and its applications, INTEC, London, UK, p. 188.
<https://www.intechopen.com/books/morphodynamic-model-for-predicting-beach-changes-based-on-bagnold-s-concept-and-its-applications>
- Uda, T. and Kawano, S. 1996. Development of a predictive model of contour line change due to waves, *Proc. JSCE*, No. 539/II-35, 121–139. (in Japanese)
- Yokota, T., Uda, T., and Noshi, Y. 2022. Numerical simulation on sand accumulation behind artificial reefs and enhancement of windblown sand to hinterland, in Numerical Simulation, INTEC, London, UK, 1–12.
<https://www.intechopen.com/online-first/numerical-simulation-on-sand-accumulation-behind-artificial-reefs-and-enhancement-of-windblown-sand->